Electron paramagnetic resonance study of defects in SiC

Patrick Carlsson

Linköping 2010

Linköping Studies in Science and Technology,
Dissertations, No. 1319

Author

Patrick Carlsson
Department of Physics, Chemistry and Biology (IFM)
Linköping University
SE-581 83 Linköping, Sweden

Cover illustration: Spectra of the LE5b and EI1 EPR centers in 6H-SiC acquired for different magnetic field directions.
by Patrick Carlsson, used with permission

Abstract

Silicon carbide (SiC) is a wide bandgap semiconductor (energy gap of 3.26 eV and 3.03 eV for 4H- and 6H-SiC, respectively). With outstanding physical and electronic properties, SiC is a promising material for high-power, high-frequency and high-temperature applications. The electronic properties of a semiconductor are to a large extent determined by point defects in the crystal. As known from other semiconductors, defect control is crucially important for the successful device applications. Point defects can be impurities, such as the shallow nitrogen (N) donor or boron acceptor (the residual n- and p-type dopants in SiC), or intrinsic defects, such as vacancies, antisites, interstitials or combinations thereof. One of the key issues in the SiC technology is to develop semi insulating (SI) SiC substrates required for SiC MEtal Semiconductor Field Effect Transistors (MESFETs) and also for III-nitride based High Electron Mobility Transistors (HEMTs), to reduce the parasitic capacitance and to improve the device performance. For achieving the SI behavior the Fermi level should be pinned near the middle of the bandgap. This can be realized using defects with deep acceptor level(s) to compensate the residual shallow N donors which cause the natural n-type doping of as-grown SiC.

Vanadium (V) doped SI SiC has been developed since the 1990s. However, SiC MESFETs using V-doped SI SiC substrates are shown to have severe problems with electron trapping to deep levels in the SI substrates which causes reduction of the drain current and instability of the device performance. Since the beginning of this decade, V-free high-purity SI (HPSI) SiC substrates using intrinsic defects to compensate the N donors have been developed. The work in this thesis has been devoted to characterize defects in HPSI SiC using electron paramagnetic resonance (EPR). EPR detects transitions between energy levels split up by the interaction of unpaired electron spins (localized at the defect and neighboring atoms) with an applied magnetic field. Thanks to the sensitivity of the electron spins to their surroundings; especially to nearby nuclear spins that further splits the energy levels by the so-called hyperfine (hf) interaction, one can extract information on the structure and electronic configuration of a defect.

The work has been focused on (i) the identification of prominent defects, (ii) the determination of their energy levels and roles in the carrier compensation processes, (iii) the defect interaction and the stability of the SI properties at high temperatures, in order to identify the optimal defect(s) to be used for controlling the SI properties. EPR and *ab initio* supercell calculations have been the main tools for defect identification and all three common polytypes 3C-, 4H- and 6H-SiC of different conducting types (n-, p-type and SI) have been investigated. For determination of the energy levels in the bandgap, the combined results of EPR and photoexcitation EPR (photo-EPR), Deep Level Transient Spectroscopy (DLTS), the temperature dependence of the resistivity, and *ab initio* calculations have been evaluated. Annealing studies up to 1600 °C for samples with different defect compositions have been carried out for obtaining knowledge on the defect interaction and thermal stability of the SI properties as well as the change in resistivity, activation energy

and defect concentration. Below is a short summary of the papers included in the thesis.

In paper 1, the identification of the neutrally charged divacancy ($V_C V_{Si}^0$) in 4H-SiC, by EPR and *ab initio* calculations, is presented. The divacancy is a common defect in SiC and it is thought to play a role in carrier compensation in HPSI SiC. Annealing studies show that it is formed during migration of carbon vacancies (V_C) and silicon vacancies (V_{Si}) and in the studied samples it is thermally stable up to at least 1500 °C.

Paper 2 presents EPR identification of prominent defects in different types of HPSI 4H-SiC substrates grown by high-temperature chemical vapor deposition (HTCVD) and physical vapor transport (PVT), the determination of some of their deep acceptor levels and their roles in carrier compensation processes. V_{Si}, V_C, carbon antisite-vacany pair ($C_{Si} V_C$), and $V_C V_{Si}$ were found to be the most common defects in different types of HPSI 4H-SiC. The samples could be grouped into three activation energy ranges E_a~0.8–0.9 eV, ~1.1–1.3 eV, and ~1.5 eV, and the possible defect levels related to these energies were discussed for each group. The samples with E_a~1.5 eV contain high concentrations of V_C and $V_C V_{Si}$ and low concentrations of V_{Si} and as these samples had the most thermally stable SI properties, due to the increased thermal stability of V_C when V_{Si} is absent, we concluded that this defect composition is preferable.

A similar study is presented in paper 4 of different types of HPSI 6H-SiC substrates grown by HTCVD. The samples could be grouped into two activation energy ranges E_a~0.6-0.7 eV and ~1.0-1.2 eV. V_C, $C_{Si} V_C$ and $V_C V_{Si}$ were found to be the prominent defects and the relationship between their energy levels and the activation energies was discussed. The materials were still SI after annealing up to 1600°C, although the activation energies were lowered. The (+|0) level of V_C was also specifically studied by photo-EPR and determined to be located at ~1.47 eV above the valence band maximum, similar to 4H-SiC.

The content of Paper 3 concerns an EPR study of two defects, labeled L5 and L6, in electron irradiated n-type 3C-SiC. The L5 defect could be related to the neutrally charged divacancy as it shows some features similar to the divacancy in 4H-SiC. The L6 defect anneals out at low temperatures (~200°C) and could possibly be carbon interstitial related.

Paper 5 presents an attempt to study the energy levels of V_C by photo-EPR without the usual interference from other defect levels. By using pure free-standing n-type 4H-SiC epilayers with very low defect concentrations and low-energy electron (200 keV) irradiation we could combine photo-EPR and DLTS to study energy levels related to V_C. V_C^+ and V_C^- could be detected simultaneously and from the study we concluded that the (+|0) level is located at ~E_C–1.77 eV and suggested that the (0|–) and (1–|2–) levels are located at ~E_C–0.8 eV and ~ E_C–1.0 eV, respectively.

The investigation in paper 6 concerns the identification of the EI4 EPR center in 4H- and 6H-SiC. Based on detailed studies of the hf interactions, the annealing behavior and *ab initio* supercell calculations we believe the corresponding defect is a complex between a carbon vacancy-carbon antisite and a carbon vacancy at the

third neighbor site of the antisite in the neutral charge state, $(V_C\text{-}C_{Si}V_C)^0$. It could be directly involved in carrier compensation in some samples before it anneals out (at ~850 °C in irradiated samples or higher temperatures in as-grown sample) and also seems to be an intermediate state in the formation of the divacancy.

In Paper 7, an EPR study of a radiation-induced defect, labeled LE5, in 4H- and 6H-SiC is presented. The observation of the LE5 spectra in samples irradiated at low temperatures (77-100 K) indicates that it is a primary defect. From the low symmetry (C_{1h}), the Si hf structures, and the low anneal-out temperature (~600-750 °C) we suggested that the defect may be a complex involving a silicon antisite (Si_C) perturbed by a nearby defect.

Populärvetenskaplig sammanfattning

Kiselkarbid (SiC) kan förekomma i många olika s.k. polytyper, beroende på hur kristallen är uppbyggd, med olika fysiska och elektriska egenskaper. Gemensamt för alla polytyper är att varje Si-atom binder till fyra C-atomer och varje C-atom binder till fyra Si-atomer i en tetraedrisk struktur. Vi har studerat polytyperna 3C-, 4H- och 6H-SiC.

Kiselkarbid är en halvledare med stort förbjudet bandgap (energigap på respektive 3,26 eV och 3,03 eV för 4H-och 6H-SiC), vilket innebär att elektronerna i bindningarna i materialet måste tillföras mycket energi för att frigöras och bli rörliga och därmed kunna leda ström. SiC är på så sätt mer likt ett elektriskt isolerande material än t.ex. kisel, som har ett litet bandgap, men samtidigt kan det dopas med främmande atomer för att bli mer elektriskt ledande, vilket är typiskt för halvledare. Med enastående fysiska och elektroniska egenskaper är kiselkarbid ett lovande material för högeffekt-, högfrekvens- och högtemperaturer-applikationer.

En av de viktigaste uppgifterna inom SiC-utvecklingen är att utveckla semiisolerande (SI) (så lite elektriskt ledande som möjligt) SiC-substrat, som krävs för att minimera parasitisk kapacitans i, och därmed förbättra prestandan på, högfrekvenstransistorer av SiC och även av andra halvledarmaterial där SiC används som bassubstrat. För att uppnå SI egenskaper bör elektronerna i bindningarna mellan atomerna ha svårt att bli rörliga. Men när man tillverkar SiC kommer det oundvikligen in främmande dopämnen som binder in i materialet på samma sätt som Si eller C men som, om de har fler elektroner i sitt yttersta skal än Si och C (4 elektroner), lätt kan släppa den extra elektron som inte får plats i någon bindning så att den kan leda ström, och om de har färre elektroner i sitt yttersta skal skapar det bindningar med en elektron för lite, s.k. hål. Dessa hål kan också lätt bli rörliga i materialet och därmed också leda ström. Kväve (N) (med fem elektroner i yttersta skalet) och bor (B) (tre elektroner) är de vanligaste oavsiktliga dopämnena i SiC. Har de samma koncentration tar extraelektronerna och hålen ut varandra men det är svårt att kontrollera och oftast är kvävekoncentrationen något högre, så man har rörliga elektroner i materialet.

Om man vill åstadkomma SI egenskaper måste man binda dessa elektroner. Det kan göras m.h.a. andra defekter i materialet som kan binda extraelektronerna till sig starkare än N-atomerna gör och som inte bidrar med lättrörliga hål om de inte tar till sig extraelektroner. Dessa defekter sägs då ha djupa acceptornivåer (till skillnad från grunda acceptornivåer som B har i SiC och grunda donatornivåer som N har i SiC). Vanadin (V) har både djupa acceptornivåer och djupa donatornivåer i SiC som kan användas för att kompensera grunda donatornivåer respektive grunda acceptornivåer. V-dopat SI SiC har utvecklats sedan 1990-talet men höga V koncentrationer krävs för SI egenskaper, då bara en del av V-atomerna är elektriskt aktiva i SiC, och brister i prestandan på transistorer med dessa substrat har påvisats.

Sedan början av det här årtiondet har istället substrat av högrent SI (HPSI) SiC, där inneboende defekter kompenserar de resterande N-donatorerna, använts mer och mer. Inneboende defekter är defekter utan främmande atomer, t.ex. vakanser

(frånvaro av Si- eller C-atom på en plats där det borde sitta en i kristallen), interstitialer (en Si- eller C-atom på en plats där det inte borde sitta någon atom), "antisites" (en Si-atom på C-atomplats eller vice versa), eller kombinationer av dessa. Dessa defekter kan också ha djupa acceptor- och/eller donator-nivåer. Kunskapen om inneboende defekter i SiC är fortfarande bristfällig och kontrollen av SI egenskaperna i HPSI SiC kan bli bättre.

Arbetet i den här avhandlingen har ägnats åt att studera främst inneboende defekter i HPSI SiC med mätmetoden Elektron Paramagnetisk Resonans (EPR). EPR detekterar övergångar mellan energinivåer som splittrats upp genom interaktionen mellan oparade elektronspin (lokaliserade på defekten och angränsande atomer) med ett pålagt magnetfält. Tack vare elektronspinnets känslighet för sin omgivning, speciellt för närliggande atomkärnspin, kan man utvinna information om en defekts struktur och elektronkonfiguration.

Arbetet har varit inriktat på att (i) fastställa vilka defekter som är framträdande i SiC, (ii) fastställa deras energinivåer och vilken roll de kan spela för SI egenskaperna, och (iii) undersöka hur defekter migrerar och interagerar i materialet och hur det påverkar stabiliteten för SI egenskaperna vid höga temperaturer. Allt i syfte att ta reda på vilka defekter som bäst kan användas för kontroll av SI egenskaperna. Tre vanliga polytyper, 3C-, 4H-och 6H-SiC, av olika slag (n-och p-typ och SI) har undersökts för att identifiera olika defekter. EPR och fysikaliska beräkningar är de främsta verktygen för detta. För bestämning av energinivåer i bandgapet har även resultat av andra, elektriska och optiska, mätmetoder varit värdefulla. Varmbehandlingsstudier upp till 1600°C har utförts på prov med olika defektkompositioner, för att öka kunskapen om defektinteraktion och termisk stabilitet för SI egenskaperna.

Table of Contents

Acknowledgements

During my five years as a PhD-student and Linköping-citizen I've been very fortunate to have such good friends and coworkers. This is my chance to thank you. So, thank you…

…**Erik Janzén**, for giving me the opportunity to be a part of the Semiconductor Materials group and to work in this interesting field, and for always being kind and supportive.

…**Nguyen Tien Son**, for always helping, supporting and patiently explaining things to me, and for setting the example of an excellent researcher.

…**Anne Henry**, **Ivan Ivanov**, and all the other coworkers in the Semiconductor Materials group, for your friendliness and for sharing your vast knowledge on SiC and semiconductor physics.

…**Eva Wibom**, **Arne Eklund** and **Sven Andersson,** for helping me out when I needed it.

…**Andreas Gällström**, for your friendship and your sarcastic humor.

…**Franziska Beyer**, **Björn Magnusson**, **Jawad ul Hassan**, **Henrik Pedersen**, **Anders Lundskog**, **Stefano Leone, Daniel Dagnelund, Arvid Larsson**, and the other PhD students in the Semiconductor Materials group, for your cooperation, nice company, and all the good times at and outside of the university.

…**Lunchklubben** and all the PhD students (and others) at IFM that I've had the pleasure of spending time with over innumerous lunches and cups of coffee, and occasional beers.

…**Salsagänget** with extensions, for making me feel that I have a life outside of the university too.

…**Vasa Wailers**, now in korpen division 1. Vasa for life!

…**My family**, always supportive, even though I seldom make the effort to explain my research for you, and too seldom come home to visit.

…**Sofie**, my love, for enduring these trying times and for always caring about us.

Included papers

1. **Divacancy in 4H-SiC**
   N.T. Son, <u>P. Carlsson</u>, J. ul Hassan, E. Janzén, T. Umeda, J. Isoya, A. Gali, M. Bockstedte, N. Morishita, T. Ohshima, and H. Itoh
   Physical Review Letter **96**, 055501 (2006)

2. **Defects and carrier compensation in semi-insulating 4H-SiC substrates**
   N.T. Son, <u>P. Carlsson</u>, J. ul Hassan, B. Magnusson, and E. Janzén
   Physical Review B **75**, 155204 (2007)

3. **Electron paramagnetic resonance study on n-type electron-irradiated 3C-SiC**
   <u>P. Carlsson</u>, K. Rabia, N.T. Son, N. Ohshima, N. Morishita, H. Itoh, J. Isoya, and E. Janzén
   Proc. of IVC-17/ICSS-13/ICN+T2007; Stockholm, Sweden; July 2-6, 2007
   J. Phys.: Conf. Ser. **100**, 042032 (2008)

4. **Intrinsic Defects in HPSI 6H-SiC; an EPR Study**
   <u>P. Carlsson</u>, N.T. Son, B. Magnusson, and E. Janzén
   Proc. of the ICSCRM2007; Otsu, Japan; October 15 - 19, 2007
   Materials Science Forum **600-603**, 381-384 (2009)

5. **Deep levels in low-energy electron-irradiated 4H-SiC**
   <u>P. Carlsson</u>, N. T. Son, F. Beyer, H. Pedersen, J. Isoya, N. Morishita, T. Ohshima, and E. Janzén
   Phys. Status Solidi – Rapid Research Letters **4**, 121-123 (2009)

6. **EPR and *ab inito* calculation study on the EI4 center in 4H- and 6H-SiC**
   <u>P. Carlsson</u>, N. T. Son, A. Gali, J. Isoya, N. Morishita, T. Ohshima, B. Magnusson, and E. Janzén
   Submitted to Physical Review B

7. **A primary complex defect in electron-irradiated 3C-, 4H- and 6H-SiC**
   <u>P. Carlsson</u>, N.T. Son, J. Isoya, N. Morishita, T. Ohshima, and E. Janzén
   Manuscript

My contributions to the papers:
For paper 1 and 2, I did some of the EPR measurements and analysis of spectra. For papers 3-7, I did most of the experimental work and analysis (in paper 3, together with K. Rabia), aided by N. T. Son when needed. The DLTS measurements in paper 5 were done by F. Beyer. The first drafts of papers 3-7 were written by me and the papers were then finalized with the help of N. T. Son and E. Janzén. A. Gali performed the *ab initio* calculations and wrote the details on that part in paper 6.

Publications not included in the thesis

Journal Articles

Deep levels and carrier compensation in V-doped semi-insulating 4H-SiC
N.T. Son, P. Carlsson, A. Gällström, B. Magnusson, and E. Janzén
Appl. Phys. Lett. **91**, 202111 (2007)

Very high crystalline quality of thick 4H-SiC epilayers grown from methyltrichlorosilane (MTS)
H. Pedersen, S. Leone, A. Henry, V. Darakchieva, P. Carlsson, A. Gällström, and E. Janzén
Phys. Status Solidi – Rapid Research Letters **2**, 188 (2008)

Conference Papers

Characterization of semi-insulating SiC
N.T. Son, P. Carlsson, B. Magnusson, and E. Janzén
Invited talk; Proc. of the MRS Spring Meeting; San Francisco, USA;
Mater. Res. Soc. Symp. Proc. **911**, 201-211 (2006)

Deep Acceptor Levels of the Carbon Vacancy-Carbon Antisite Pairs in 4H-SiC
P. Carlsson, N.T. Son, T. Umeda, J. Isoya, and E. Janzén
Proc. of the ECSCRM2006; Newcastle, UK; September 4-8, 2006
Mater. Sci. Forum, **556-557**, 449-452 (2007)

Influence of Cooling Rate after High Temperature Annealing on Deep Levels in High-Purity Semi-Insulating 4H-SiC
A. Gällström, P. Carlsson, B. Magnusson, A, Henry, N. T. Son, and E. Janzén
Proc. of the ECSCRM2006; Newcastle, UK; September 4-8, 2006
Mater. Sci. Forum **556-557**, 371-375 (2007)

Intrinsic Defects in Semi-Insulating SiC: Deep Levels and Their Roles in Carrier Compensation
N.T. Son, P. Carlsson, B. Magnusson, and E. Janzén
Proc. of the ECSCRM2006; Newcastle, UK; September 4-8, 2006
Mater. Sci. Forum **556-557**, 465-468 (2007)

Prominent defects in semi-insulating SiC substrates
N. T. Son, P. Carlsson, A. Gällström, B. Magnusson, and E. Janzén
Invited talk at the 24th International Conference on Defects in Semiconductors;
Albuquerque, New Mexico, USA; July 21-27, 2007
Physica B **401-402**, 67-72 (2007)

Contact-Less Electrical Defect Characterization of Semi-Insulating 6H-SiC Bulk Material
S. Hahn, F. Beyer, A. Gällström, P. Carlsson, A. Henry, B. Magnusson, J. Niklas, and E. Janzén
Proc. of the ICSCRM2007; Otsu, Japan; October 15 - 19, 2007
Mater. Sci. Forum **600-603**, 405-408 (2009)

Deep levels responsible for semi-insulating behavior in vanadium-doped 4H-SiC substrates
N.T. Son, P. Carlsson, A. Gällström, B. Magnusson, and E. Janzén
Proc. of the ICSCRM2007; Otsu, Japan; October 15 - 19, 2007
Mater. Sci. Forum **600-603**, 401-404 (2009)

Photo-EPR studies on low-energy electron-irradiated 4H-SiC
P. Carlsson, N.T. Son, H. Pedersen, J. Isoya, N. Morishita, T. Ohshima, H. Itoh, and E. Janzén
Proc. of the ECSCRM2008; Barcelona, Spain; September 7-11, 2008
Mater. Sci. Forum **615-617**, 81-84 (2009)

The Silicon vacancy in SiC
E. Janzén, A. Gali, P. Carlsson, A. Gällström, B. Magnusson, and N. T. Son
Proc. of the ECSCRM2008; Barcelona, Spain, 2008
Mater. Sci. Forum **615-617**, 347-352 (2009)

The silicon vacancy in SiC
E. Janzén, A. Gali, P. Carlsson, A. Gällström, B. Magnusson and N.T. Son
Physica B: Condensed Matter 404, 4354-4358 (2009)

The carbon vacancy related EI4 defect in 4H-SiC
N.T Son, P. Carlsson, J. Isoya, N. Morishita, T. Ohshima, B. Magnusson, and E. Janzén
Proc. of the ICSCRM2009; Nürnberg, Germany; October 11 - 16, 2009
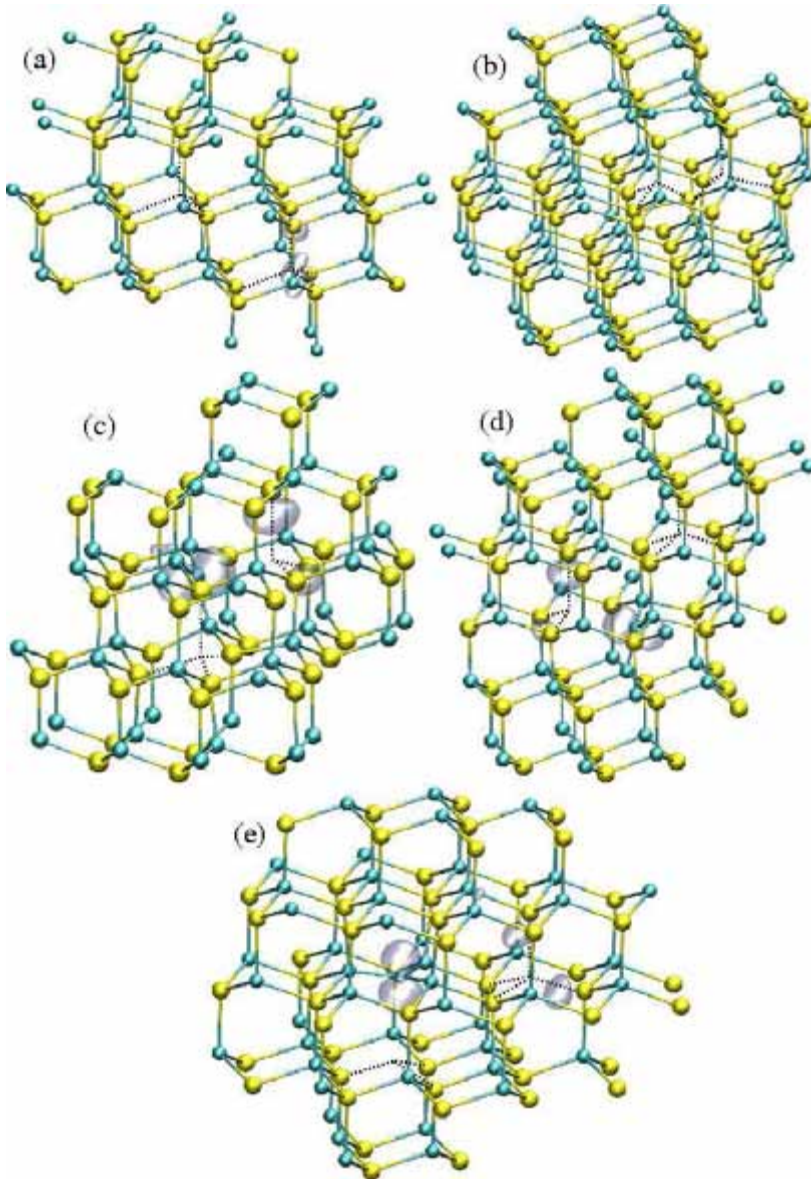Mater. Sci. Forum **645-648**, 399-402 (2010)

The EI4 center in 6H-SiC
P. Carlsson, N. T. Son, N. Morishita, T. Ohshima, J. Isoya, and E. Janzén
Proc. of NSM 23; Reykjavik, Iceland, 2009
Accepted for Physica Scripta T

FIG. 9. (Color online) The defect configurations considered by our *ab initio* calculations. The clusters are cut from the 576-atom supercell showing the optimized geometry of the defects. (a) The far distance V_C-V_C pair. Next, different configurations of V_C and $C_{Si}V_C$ pair: (b) V_C approached by V_C part of $C_{Si}V_C$ pair; (c) V_C approached by C_{Si} part of $C_{Si}V_C$ pair where $C_{Si}V_C$ pair is off-axis and the symmetry is C_1; (d) V_C approached by C_{Si} part of $C_{Si}V_C$ pair where $C_{Si}V_C$ pair is off-axis and the symmetry is C_{1h}; (e) V_C approached by C_{Si} part of $C_{Si}V_C$ pair where $C_{Si}V_C$ pair is on-axis and the symmetry is C_{1h}. The carbon (silicon) atoms are depicted as cyan (yellow) balls. The dotted lines guide the eyes to find the vacant sites in the complex. The iceblue lobes are the isosurfaces of the calculated spin density for S=1 ground state systems.

Thus, this complex may be detected in SiC but it is not responsible for the EI4 EPR center. Finally, we note that it cannot be disregarded that the C_1 symmetry configuration depicted in Fig. 9(c), which has a very similar spin density distribution to that of the C_{1h} symmetry configuration depicted in Fig. 9(d), can be detected by EPR without any excitation. In summary, the configuration depicted in Fig. 9(d) shows the features (symmetry *and* spin density distribution) that may explain the experimental findings about the EI4 EPR center, thus we investigated this configuration of the V_C-$C_{Si}V_C$ complex in detail.

Despite that the V_C-$C_{Si}V_C$ complex has a relatively low symmetry, the combination of the single particle orbitals coming from the approached V_C and from $C_{Si}V_C$ can form near degenerate states because both isolated defects possess defect levels at very similar energies in the fundamental band gap. That is the source of the stabilization of the high spin ground state. The detailed spin density distribution of the V_C-$C_{Si}V_C$ complex is shown in Fig. 10. The largest localization can be found on a single Si dangling bond which points near parallel to the *c* axis of the crystal. The spin density is also well localized on the off-axis C_{Si} dangling bond pointing to the vacant site. The direction of the **g** tensor and the **D** tensor is largely influenced by these dangling bonds making their largest component off-axis. Those atoms that cause larger hyperfine splitting than 10 G, in addition to the single Si and the C_{Si} mentioned above, are depicted by red color. Experimentally, we found the sets of 2-2-1 Si atoms in this region which is in excellent agreement with the observed data (see Table I). The blue colored atoms exhibit hyperfine splitting close to 5 G and could be the main cause of the innermost detectable hf structure, shown in Fig. 6. Overall, the calculated hyperfine tensors are in good agreement with the resolved hyperfine data and the calculations consistently yield the unresolved hyperfine constants.

The EI4 EPR center may be identified by the particular C_{1h} configuration of the V_C-$C_{Si}V_C$ complex shown in Fig. 10. We found that the (+|0) and (0|-) occupation levels are at about 1.6 eV and 2.0 eV above the valence band, respectively, which shows that this defect is indeed neutral at the position of the Fermi-level where the isolated V_C is neutral and the isolated V_{Si} is negatively charged[36]. This is in line with the scenario we gave above about the possible formation routes of the EI4 center. The calculated binding energy of this complex with respect to the isolated carbon and silicon vacancies is over 3 eV favoring the complex formation, which explains the stability of this complex. According to the experimental finding, this complex should transform to divacancy after higher temperature anneal, thus this issue must be studied for unambigouos identification of this defect. We find a transition route where the migrating C_{Si} atom can jump from its original position in the V_C-$C_{Si}V_C$ complex to the vacant site of the approached V_C, resulting in the divacancy complex. The transition state and other important configurations during this conversion are shown in Fig. 11. The migrating C_{Si} first temporarily binds to the Si-atom possessing the largest hyperfine interaction in the V_C-$C_{Si}V_C$ complex beside the two neighbor C atoms and two originally low-coordinated Si-atoms of the approached V_C part of the complex, releasing one neighbor C atom (Fig. 11(b)). The bonds between Si-atoms and the

18
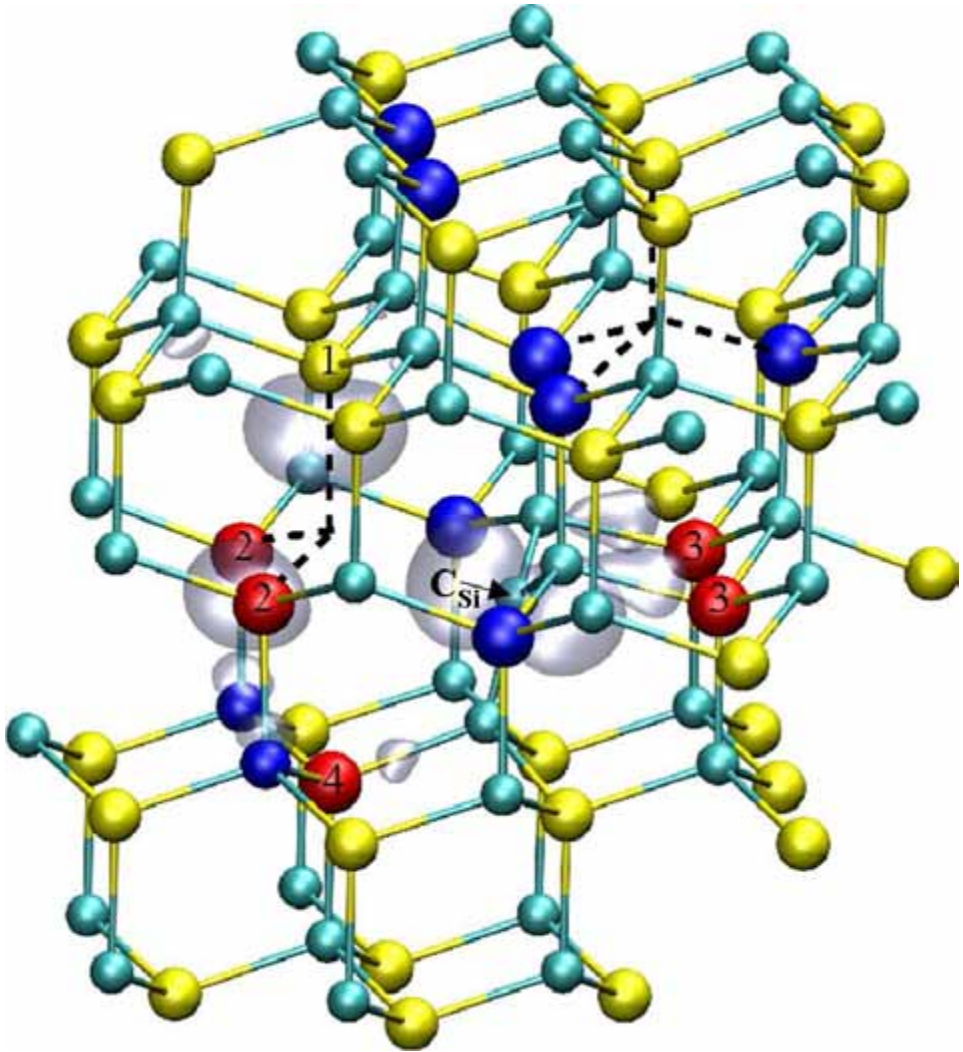
FIG. 10. (Color online) The suggested defect model for the EI4 center in the 4H-SiC crystal structure. The cluster is cut from the 576-atom supercell showing the optimized geometry of the defect. Most of the carbon (silicon) atoms are depicted as cyan (yellow) balls. The dotted lines guide the eyes to find the vacant sites in the complex. The iceblue lobes are the isosurfaces of the calculated spin density. The atoms most important for the detected hf structure are indicated by 1-4 which should read as Si_{1-4} atoms. The C_{Si} atom binds to three other C atoms in the middle of the figure. The red balls show those Si atoms that have larger hyperfine splitting than 10 G while blue balls show those Si and C atoms that have about 5 G hyperfine splitting.

migrating C_{Si} keeps the total energy of the system relatively low. Then the migrating C_{Si} wanders to the side of the approached V_C by releasing the Si-atom in the $C_{Si}V_C$ part of the complex (Fig. 11(c)) and during this action one finds the transition state shown in Fig. 11(d). The migrating C atom leaves a V_{Si} behind, near to the V_C which was originally part of the $C_{Si}V_C$ pair. The migrating C atom goes further to the nearest vacant site without any barrier energy (Fig. 11(e)), and finally forms the divacany (Fig. 11(f)). The calculated energy barrier of this process is about 3.1 eV which is larger than the migration barrier energy of V_{Si} but smaller than the migration barrier energy of V_C at the relevant charge states. The reverse process has more than 4.7 eV energy barrier which is a higher energy than that for migration of V_C, thus the reverse process is not likely to occur. These findings are very consistent with the experimental data: at lower temperature anneal (<750 °C) V_C is stable and the migrating V_{Si} can form the V_C-$C_{Si}V_C$ complex with V_C, while at higher temperature anneal the complex can transform directly to a divacancy which remains stable. This result implies that the immediate $V_CC_{Si}V_C$ complex, studied by Gerstmann and co-workers[22], may not form since the V_C-$C_{Si}V_C$ complex can transform directly to a divacancy.

In summary, the stability and the spin density distribution of the neutral V_C-$C_{Si}V_C$ complex, where $C_{Si}V_C$ pair is off-axis, can both explain the observed properties of the EI4 EPR center. Nevertheless, the conversion of this defect to the divacancy can only account for the formation of the P7 EPR center (off-axis divacancy), while both the P6 (on-axis divacancy) and the P7 signals enhanced in the annealing study. As mentioned earlier the EI4 EPR spectrum with off-axis **g**- and **D**-tensors is accompanied by another EPR center (EI4 axial in Fig. 2) with S=1 state and on-axis **g**- and **D**-tensors. This EPR center might be associated with the complex of on-axis $C_{Si}V_C$ pair and V_C in Fig. 10(e) and it may explain the formation of additional P6 centers upon annealing since it anneals out simultanouosly with the EI4 center. Other configurations of the V_C-$C_{Si}V_C$ complex (like shown in Fig. 9(b)) with singlet ground states can also contribute to this process where only the final product, the divacancy, can be detected by EPR.

IV. SUMMARY

Using electron-irradiated HPSI 4H- and 6H-SiC samples, we were able to observe a strong signal of the EI4 EPR-center, including an additional large-splitting hf structure due to the interaction with one Si, a smaller-split hf structure due to the interaction with one C atom, and other hf structures related to the interaction with a number of Si atoms. Based on the observed hf structures, defect symmetry and annealing behavior, together with results from supercell calculations, we suggest that the defect corresponding to the EI4 EPR-center in 4H- and 6H-SiC is a neutrally charged complex consisting of a carbon antisite-vacancy pair in off-axis configuration and another carbon vacancy at the third nearest neighbor site of the antisite, V_C-$C_{Si}V_C$, with both vacancies and the antisite in the $(11\bar{2}0)$ or equivalent plane.
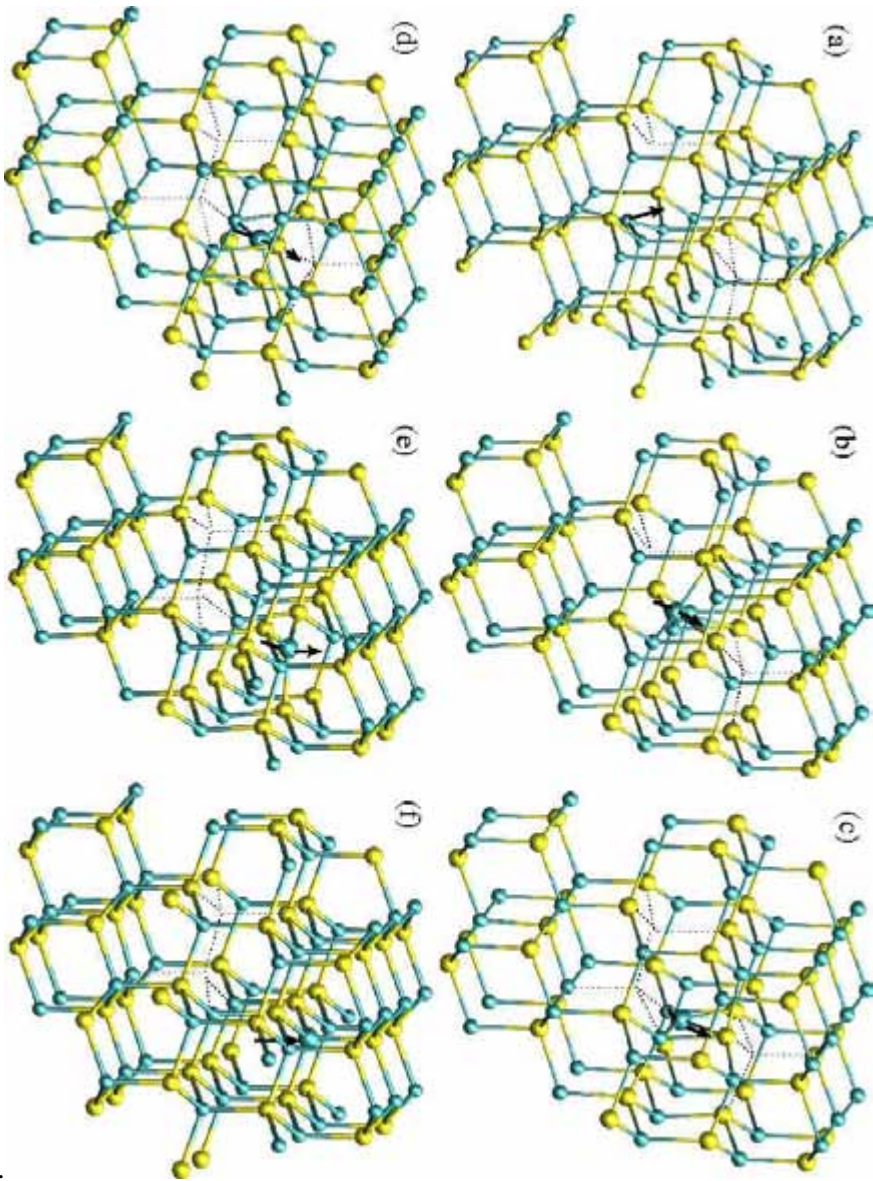
FIG. 11. (Color online) The suggested model of the transition from EI4 center to the off-axis divacancy. The clusters are cut from the 576-atom supercell showing the calculated geometry of the defects using the nudged elastic band method. (a) starting configuration: optimized V_C-$C_{Si}V_C$ defect, (b) migrating C_{Si} in the $C_{Si}V_C$ part of the complex, (c) migrating C_{Si} toward the approached V_C part of the defect, (d) transition state, (e) migrating C atom toward the nearest vacant site, (f) final configuration: optimized divacancy. The carbon (silicon) atoms are depicted as cyan (yellow) balls. The dotted lines guide the eyes to find the vacant sites in the complex. The arrow indicates the movement of the migrating atom.

21

ACKNOWLEDGEMENTS

References

[1] N. T, Son, P. N. Hai, A. Shuja, W. M Chen, J. L. Lindström, B. Monemar, and E. Janzén, Mat. Sci. Forum **338-342**, 821 (2000).

[2] V. S. Vainer and V.A. Ilin, Sov. Phys. Solid State **23**, 2126 (1981).

[3] V. S. Vainer, V. I. Veinger, V. A. Ilin, and V. F. Tsvetkov, Sov. Phys. Solid State **22**, 2011 (1980).

[4] A. Ellison, B. Magnusson, C. Hemmingsson, W. Magnusson, T. Iakimov, L. Storasta, A. Henry, N. Henelius, and E. Janzén, Mater. Res. Soc. Symp. Proc. **640**, H1.2 (2001).

[5] A. Ellison, B. Magnusson, N. T. Son, L. Storasta, and E. Janzén, Mater. Sci. Forum **433-436**, 33 (2003).

[6] A. Ellison, B. Magnusson, B. Sundqvist, G. Pozina, J. P. Bergman, E. Janzén, and A. Vehanen, Mater. Sci. Forum **457-460**, 9 (2004).

[7] St. G. Müller, M. F. Brady, W. H. Brixius, R. C. Glass, H. McD. Hobgood, J. R. Jenny, R. T. Leonard, D. P. Malta, A. R. Powell,V. F. Tsvetkov, S. T. Allen, J. W. Palmour, and C. H. Carter, Jr., Mater. Sci. Forum **433-436**, 39 (2003).

[8] J. R. Jenny, D. P. Malta, M. R. Calus, St. G. Müller, A. R. Powell, V. F. Tsvetkov, H. McD. Hobgood, R. C. Glass, and C. H. Carter, Jr., Mater. Sci. Forum **457-460**, 35 (2004).

[9] N. T. Son, P. Carlsson, J. ul Hassan, B. Magnusson, and E. Janzén, Phys. Rev. B **75**, 155204 (2007).

[10] P. Carlsson, N. T. Son, B. Magnusson, and E. Janzén, Mat. Sci. Forum **600-603**, 381 (2009).

[11] T. Umeda, N. T. Son, J. Isoya, E. Janzén, T. Ohshima,N. Morishita, H. Itoh, A. Gali, and M. Bockstedte, Phys. Rev. Lett. **96**, 145501 (2006).

[12] N. T. Son, P. N. Hai, and E. Janzén, Phys. Rev. B **63**, 201201(R) (2001).

[13] T. Umeda, J. Isoya, N. Morishita, T. Ohshima, T. Kamiya, A. Gali, P. Deák, N. T. Son, and E. Janzén, Phys. Rev. B **70**, 235212 (2004).

[14] J. Isoya, T. Umeda, N. Mizuochi, N.T. Son, E. Janzén, and T. Ohshima, Phys. Stat. Sol. (b) **245**, 1298-1314 (2008).

[15] E. Sörman, N. T. Son, W. M. Chen, O. Kordina, C. Hallin, and E. Janzén, Phys. Rev. B **61**, 2613 (2000).

[16] E. Janzén, A. Gali, P. Carlsson, A. Gällström, B. Magnusson, and N. T. Son, Physica B **404**, 4354 (2009)

[17] B. Bleaney and R. S. Rubins, Proc. Phys. Soc. **77**, 103 (1961)

[18] J. R. Morton and K. F. Preston, J. Mag. Res. **30**, 577 (1978).

[19] Th. Lingner, S. Greulich-Weber, J-M. Spaeth, U. Gerstmann, E. Rauls, Z. Hajnal, Th. Frauenheim, and H. Overhof, Phys. Rev. B **64**, 245212 (2001).

Introduction to the field

*Silicon Carbide and Electron Paramagnetic Resonance*

1   Silicon Carbide

Silicon carbide (SiC) was first discovered by Jöns Jacob Berzelius in 1824 [1] and moissanite, the mineral form of SiC, was discovered by Henri Moissan in a meteor crater in 1893 [2]. Edward G. Acheson started producing SiC as an abrasive material in 1894 [3]. With the later interest of SiC as a semiconductor came the desire to grow large high-quality single crystals, and thanks to milestone developments by Lely in sublimation growth (1955) [4], Tariov and Tsvetkov in seeded sublimation growth (1978) [5], Matsunami in epitaxial growth (1981) [6], and the work of many others, high-quality substrates and some SiC power devices are today commercially available.
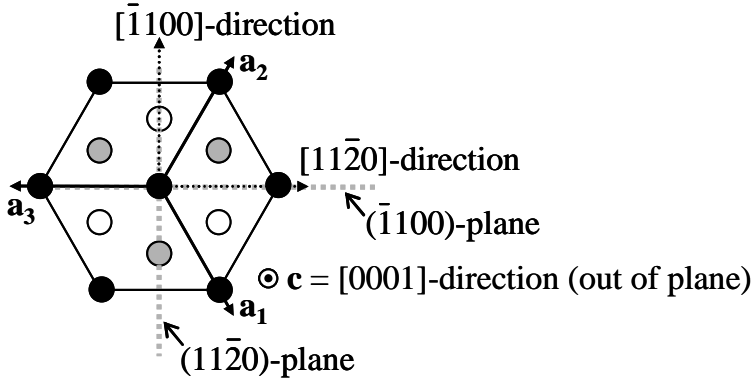
1.1 Crystal structure

An interesting feature of SiC is its polytypism, which implies that SiC exists in many different polytypes, differing in the stacking sequence of Si-C bilayers. There are more than 250 known polytypes of SiC [7] but in this thesis we focus mainly on three most common and technologically important polytypes: 3C, 4H, and 6H. The polytypes can be described as different stacking sequences of identical crystal planes, as illustrated in Figure 1.1. Each plane is a bilayer where each point in Figure 1.1 symbolizes one Si-atom on top of one C-atom, or vice versa. The polytypes are denoted by a number, specifying the number of planes stacked before the stacking sequence repeats, and a capital letter, symbolizing the resulting structure of the crystal: C-cubic, H-hexagonal, R-rhombohedral [8].
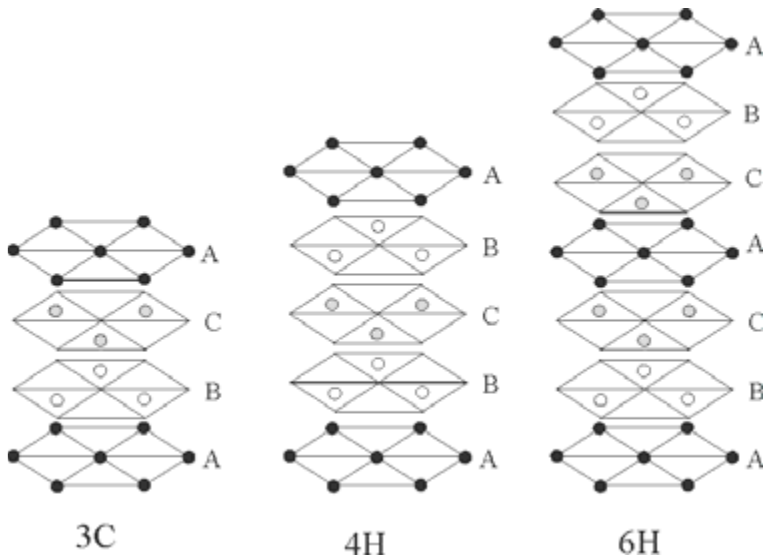

Figure 1.1 The stacking sequences of 3C-, 4H-, and 6H-SiC.

The crystal structure of 3C-SiC is the cubic zincblende structure while the stackings in 4H- and 6H-SiC give rise to hexagonal structures. To describe the crystal planes and directions in a hexagonal lattice, four (instead of three as for a cubic lattice) Miller indices, related to the crystal axes $\mathbf{a_1}$, $\mathbf{a_2}$, $\mathbf{a_3}$ and $\mathbf{c}$, are used. These are specified in Figure 1.2 where a unit cell seen along the c-axis is shown. The three *a*-axes are in the basal plane and the *c*-axis ([0001]-direction) is perpendicular to this plane (up in Figure 1.1, straight out in Figure 1.2). The Si-C bond length is 1.89 Å and the distance between adjacent Si- (or C-) atoms is the lattice constant (the side of the hexagon in Figure 1.2) *a*=3.08 [9].

Figure 1.2 The crystal axes of a hexagonal lattice: a_1, a_2, a_3 and c. Denoted by Miller indices are three high symmetry directions, [11$\bar{2}$0], [$\bar{1}$100] (dashed arrows) and [0001], and the three {11$\bar{2}$0} planes (grey dashed lines).

3C-SiC has the zincblende structure and all the sites in each sublattice (Si or C) are equivalent. In 4H- and 6H-SiC there are inequivalent sites for the atoms in the bilayers depending on where in the stacking sequence they are. This is illustrated in Figure 1.3 where the crystal structures of 4H- and 6H-SiC are shown. 4H-SiC is said to have 50% hexagonality since the arrangement of bonds follows the hexagonal wurtzite structure for half of the sites and the zincblende structure for the other half. Since the overall structure is hexagonal, the latter sites are called quasi-cubic. Similarly, 6H-SiC has 33% hexagonality and it has one hexagonal site (*h*) and two inequivalent quasi-cubic sites (k_1 and k_2).
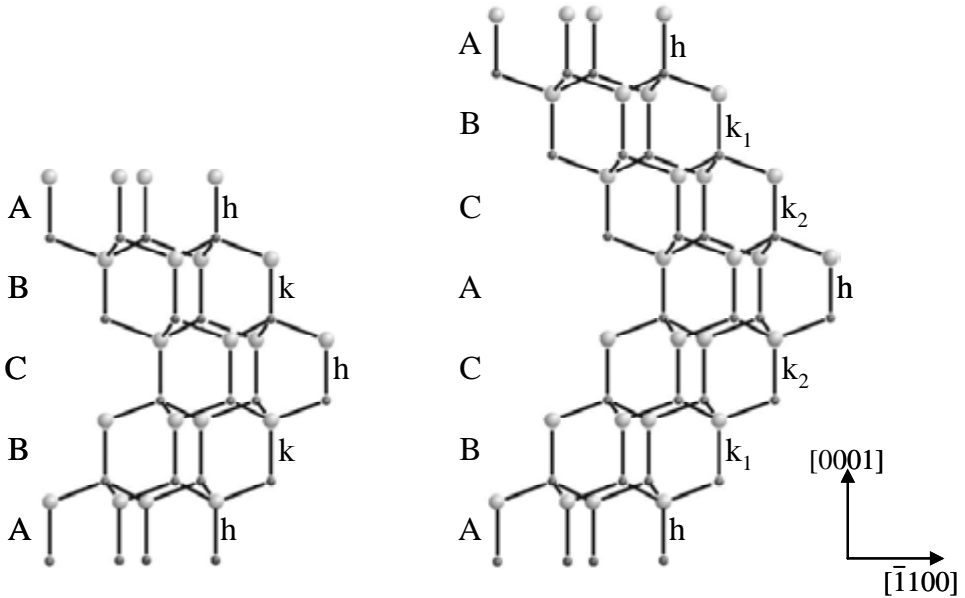
Figure 1.3 The crystal structure of 4H- and 6H-SiC. The bilayer stacking sequence is given by the capital letters, hexagonal sites by h, and quasi-cubic sites by k. In 6H-SiC there are three inequivalent lattice sites: one hexagonal site, h, and two quasi-cubic sites, k_1 and k_2.

The same defect situated on different inequivalent lattice sites can have different electronic properties, which can complicate defect studies in 4H- and 6H-SiC. Comparing the properties of the same defect in different polytypes, especially in 3C-SiC with cubic crystal structure, can facilitate the defect identification.

1.2 Properties of SiC

SiC is a wide bandgap semiconductor that can withstand a large electric field, making it suitable for high voltage applications. With large bandgap it can be operated at high temperatures without excessive leakage current and its very high thermal conductivity enables efficient cooling of devices. SiC is also a very hard and chemically inert material and hence is suitable for applications such as for sensors in harsh environments [10--12].

In Table 1.1 some important electronic properties are stated for the two most common SiC polytypes, 4H and 6H, and for some other semiconductors that could be seen as competitors for the same applications. (The values vary somewhat in the literature [13--19].)

Table 1.1 Electrical and physical properties of SiC and some other semiconductors [18,19].

	Band gap (eV)	Breakdown electric field (10^5 V/cm)	Saturated electron drift velocity (10^6 cm s^{-1})	Thermal conductivity (W cm^{-1} K^{-1})
4H-SiC	3.26	30	20-30	5-7
6H-SiC	3.08	24	21	5-7
Si	1.1	3	10	1.5
GaAs	1.43	6	10	0.45
GaN	3.45	14	22	1.3
Diamond	5.45	100	27	14-22
AlN	6.2	-	15	2

1.3 Intrinsic defects in SiC

A SiC crystal is not perfect and always contains defects, both structural defects like micropipes, edge and screw dislocations, and point defects such as impurities and intrinsic defects. SiC is a compound material and hence intrinsic defects can be isolated vacancies, interstitials, antisites and combinations of these. Since the work of this thesis mainly concerns intrinsic defects in 4H- and 6H-SiC some of the most common and important of these will now be discussed.

Taking away one carbon atom leaves a carbon vacancy (V_C) in the lattice. In the unrelaxed vacancy the four nearest neighbor (NN) Si atoms will have dangling bonds pointing toward the vacant site. The symmetry of the defect is then the same as for the lattice, with Schönflies notation [20]: C_{3v} (threefold rotational symmetry about the c axis and three mirror planes: the $(11\bar{2}0)$ and equivalent planes). Two undegenerate and one doubly degenerate one-electron state, described by linear combinations of the dangling bonds [21], can be resonant with the valance- or conduction-band or fall within the bandgap. During relaxation the energy is lowered as the long dangling bonds of Si form pair-wise bonds by so called Jahn-Teller (JT) distortion, which lowers the symmetry to C_{1h} [22] (onefold rotational symmetry and one mirror plane) and the one-electron states are transformed to four undegenerate states [21]. According to calculations, the crystal field in the hexagonal lattice complicates this and the result is pseudo-JT distortion with different bond formations for the k- and h-sites, where the h-site vacancy can still have C_{3v} symmetry after relaxation [22]. V_C has been identified by EPR and *ab initio* calculations in its positive [23--25] and negative [26] charge states, and these distortions have been experimentally verified [26,27]. At elevate temperatures the symmetry of V_C at the k-site changes from C_{1h} to C_{3v} due to thermal motional average between the bonds [26,27].

In the silicon vacancy (V_{Si}), C dangling bonds are short and do not overlap with each other to form reconstructed bonds. In this case, the exchange interaction between electrons in degenerate states is strong and the vacancy can overcome a JT distortion. Therefore, C_{3v} symmetry is kept during relaxation [22,28--30]. With strong exchange interactions, electrons prefer parallel spins resulting in high-spin

ground states for all the charge states of V_{Si} (neutral, negative and double negative) in 4H-SiC [28,29]. V_{Si} has been observed by EPR in 4H- [31] and 6H-SiC [32], and the high-spin state has been identified by EPR and electron nuclear double resonance (ENDOR) [31] and *ab initio* calculations [28,29] in its negative charge state ($S=3/2$).

The divacancy ($V_C V_{Si}$) consists of two nearest neighbor vacancies. Depending on what lattice sites the vacancies are situated on it can have several configurations (in 4H-SiC: $V_C(k)V_{Si}(k)$, $V_C(h)V_{Si}(h)$, $V_C(k)V_{Si}(h)$ and $V_C(h)V_{Si}(k)$). V_C and V_{Si} each have three NN atoms with dangling bonds. In neutral charge state the V_{Si} part of the defect is more occupied by electrons than the V_C part due to the higher electronegativity of C, and for paramagnetic states the spin density is mainly on the V_{Si} part. However, for highly negatively charged states (3–) the spin density is found to be mainly on the V_C part [21]. Similar to V_{Si}, the C_{3v} symmetry can be preserved for some charge states under relaxations for the axial (along the *c*-axis) configurations (*kk* and *hh*) and the high-spin states can be ground states. The off-axis (*hk* and *kh*) configurations naturally have C_{1h} symmetry. The identification of the P6 and P7 EPR centers ($S=1$) in 4H-SiC [33] as the neutral divacancy in axial and off-axis configurations, respectively, is presented in Paper 1 [34] of this thesis.

The carbon antisite-vacancy pair ($C_{Si}V_C$) is a stable or metastable (depending on the location of the Fermi level) [35,36] counterpart of V_{Si}, created as a neighboring C atom is trapped into V_{Si}. The pair exists in several configurations, similar to $V_C V_{Si}$. The $C_{Si}V_C$ pair is similar to V_C except that it has one of the four NN Si atoms replaced by a C atom. The off-axis configurations have C_{1h} symmetry and the axial configurations, like for V_C, can be pseudo-JT distorted to C_{1h} symmetry. $C_{Si}V_C$ has been identified by EPR and *ab initio* calculations in its positive ($S=1/2$) [37] and negative ($S=1/2$) [38] charge states. For $C_{Si}V_C^-$ only the axial configurations were identified and were shown to have a thermal motional average C_{3v} symmetry that is lowered to C_{1h} at temperatures below ~60 K [38].

Some of the ionization energies corresponding to the different charge states of these intrinsic defects have been determined by the combined results of EPR and photoexcitation EPR (photo-EPR), Deep Level Transient Spectroscopy (DLTS), temperature dependence of the resistivity and *ab initio* calculations [39,40]. Calculations of the ionization energies of vacancies and vacancy-related defects have so far been reported only for 4H-SiC [28,30,38]. The determination of vacancy-related levels using photo-EPR is discussed in Section 2.4. Although, DLTS is not applicable in high-resistivity material, once the defect levels are identified they can be studied in n- or p-type samples. The determination of the defect levels is more reliable with combining data obtained from DLTS, EPR and *ab initio* calculations as shown in Paper 5.

1.4 Semi insulating SiC

Some of the work in this thesis concerns defect control in high-purity semi-insulating (HPSI) SiC. Semi-insulating (SI) SiC substrates are required to reduce the parasitic capacitance and thereby improve the device performance of SiC MEtal Semiconductor Field Effect Transistors (MESFETs) and also of III-nitride based High Electron Mobility Transistors (HEMTs), where SiC is the best foreign substrate that is used due to the lack of native substrates. A schematic picture of a MESFET is shown in Figure 1.4.
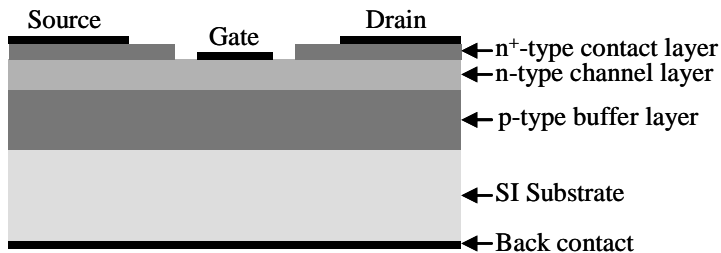
Figure 1.4 Schematic of a MESFET structure.

Between the metalized backside and the contacts on the epitaxial side of a device there is a passive parasitic capacitance, which degrades the device performance at high frequencies. For a narrow frequency bandwidth this can be compensated by an inductance adjusted for the frequency of use. For high frequency wide bandwidth devices the parasitic capacitance has to be minimized using a SI substrate. For achieving the SI behavior, the Fermi level should be pinned near the middle of the bandgap. This can be realized using deep level defects that can compensate the shallow donors and acceptors in the material. The drawback of introducing deep levels in the substrate is that they can also work as electron traps, degrading the electrical performance of the device. Defects used for controlling the SI properties in SI SiC substrates should also be thermally stable at the high temperatures (1550-1600 °C) used to grow device structures.

In many semiconductors, suitable transition metals have been used as deep level defects for SI properties and in SiC the transition metal of choice has been vanadium (V). V has a deep single acceptor level and a deep single donor level in 4H- and 6H-SiC, hence it can compensate both shallow donors and acceptors, and V doped SI SiC has been developed since the 1990s [41]. However, SiC MESFETs using V-doped SI SiC substrates are shown to have severe problems with electron trapping to deep levels in the SI substrates which causes reduction of the drain current and instability of the device performance [42]. Also, high V-doping concentrations ($\geq 10^{17}$ cm^{-3}) are required for achieving thermally stable SI properties [43], probably due to the low electrical activation of vanadium in SiC [44]. It has been shown that in SiC substrates with lower V concentrations the SI properties actually depend on deep levels of intrinsic defects [43].

Due to the problems with V-doped substrates and in order to minimize the electron trapping by deep levels the trend of the last decade has been to grow HPSI substrates, with low residual dopant concentrations, and compensate the shallow dopants using intrinsic defects with energy levels deep in the band gap. In these substrates the concentrations are typically in the mid to high 10^{15} cm^{-3} range for the most abundant shallow donor, nitrogen (N), and low 10^{15} cm^{-3} range for the most abundant shallow acceptor, boron (B) [45--49]. The substrates are thus low-doped n-type so intrinsic defects with deep acceptor levels are required for SI properties. Several different activation energies have been measured on these HPSI substrates [39,40,46,48,49], indicating that several different defect levels are involved in the carrier compensation. It is therefore important to have a good understanding of the properties of the different intrinsic defects, to be able to tailor-make HPSI substrates with desired properties. To a certain level, the introduction of the Si vacancy, C vacancy and their associated defects can be selectively controlled by growth parameters such as growth temperature, post-growth heat treatment, Si/C ratio in precursor gases, and the growth rate.

Vacancy-related defects such as V_C, V_{Si}, $V_C V_{Si}$ and $C_{Si} V_C$ were found to be prominent defects that play important roles in carrier compensating processes in HPSI 4H- and 6H-SiC, grown by physical vapor deposition (PVT) or high-temperature chemical vapor deposition (HTCVD) [39,40,46].

2 Electron Paramagnetic Resonance

EPR has, since Yevgeny Konstantinovich Zavoisky detected the first EPR spectrum in 1944 [50,51], become a powerful tool for studies in a wide range of research fields, from biology, chemistry and medicine to physics. In solid state physics it has been one of the most successful techniques for identification of paramagnetic species and their electronic structures. This brief description aims at providing the reader with the basic theory of EPR and an idea of how the spectra are analyzed and what information can be extracted by the technique. The focus is on aspects of interest for investigation of point defects in SiC.

2.1 Principle of EPR

An electron in an atom possesses electron spin, with spin angular momentum vector **s** and quantum number s=1/2, and possible orbital angular momentum, with orbital angular momentum vector **l** and quantum number l (l=0 for electrons in *s*-orbital, l=1 in *p*-orbitals, etc.). In light atoms the electron-electron interaction is stronger than the spin-orbit interaction and the total spin vector **S** is the vector sum of the **s**'s of the electrons while the total orbital angular momentum **L** is the vector sum of the **l**'s. The total angular momentum is then **J**=**L**+**S**, with quantum number J = |L-S|, |L-S|+1, ..., L+S. Due to the negative charge of the electron this angular momentum gives rise to a magnetic moment **m** = -gμ_B**J** where μ_B = e$\hbar$/2m$_e$ = 5.788×10^{-5} eV/T is the Bohr magneton and h is the Planck constant. The g-value is the spectroscopic splitting factor given by the Landé formula:

$$g \approx 1 + \frac{J(J+1) - L(L+1) + S(S+1)}{2J(J+1)} \qquad (1)$$

Under an external magnetic field, **B**, the energy levels of this magnetic moment are split up. With **B** set along the *z*-direction the hamiltonian is H=-**mB**= gμ_B**BJ**= gμ_BBJ$_z$ and the energy levels are E=gμ_BBM$_J$, where M$_J$=-J, -J+1, …, J, are the eigenvalues of J$_z$, specifying the discrete set of possible projections of **J** on the *z*-direction. This is the Zeeman effect [52] and in EPR, transitions between these energy levels are induced and detected by electromagnetic radiation in the microwave range. The transitions are induced due to a resonance phenomenon. An electron magnetic dipole affected by an external magnetic field will, as will any magnetic dipole, precess around the magnetic field direction with a frequency called the Larmor frequency, ν_L, which is proportional to the magnetic field strength, B, according to:

$$\nu_L = -g\mu_B B/h \qquad (2)$$

The projection of the magnetic moment on the external magnetic field set along the *z*-direction is specified by the quantum state as discussed above, while the *x* and *y* components oscillate with frequency ν_L. Resonance with another applied oscillating

magnetic field in the *xy*-plane and with the same frequency, ν_L, can stimulate transitions between the spin states. The spin "flips" from one state to another and a quantum of energy $h\nu_L$ is absorbed or emitted depending on if the initial state has lower or higher energy than the final state.

The simplest case is if we assume free single electrons with zero orbital angular momentum where only the intrinsic spin gives a magnetic moment. The total angular momentum is then only the spin S=1/2 and the magnetic quantum number, determining the projection of the momentum on a given direction, is $M_S=\pm 1/2$. The interaction between the external magnetic field and the electron magnetic moment splits the energy level of the electron into two levels corresponding to two possible spin states with the magnetic moment either parallel ($M_S=-1/2$) or antiparallel ($M_S=+1/2$) to the field, as shown in Figure 2.1.
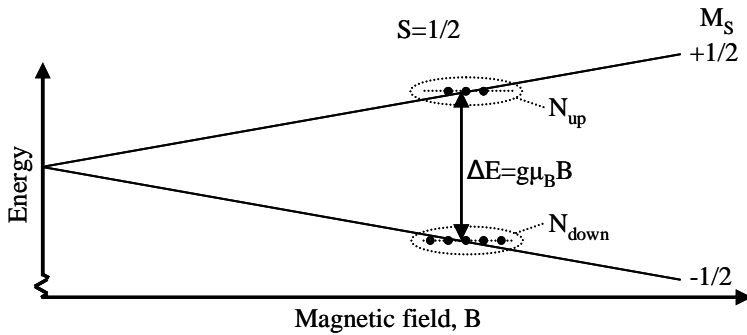
Figure 2.1 The energy levels of a spin S=1/2 paramagnetic center under a magnetic field.

The splitting between the energy levels of $M_S=+1/2$ and $M_S=-1/2$ is $g_e\mu_B B$, where $g_e=2.0023$ is the g-value for a free electron. For electrons in a solid, the splitting can be dependent on the direction of the magnetic field and g is a tensor.

The splitting between the two levels is dependent on the magnetic field strength and the g-value ($\Delta E = g\mu_B B$) and the transition between the levels can be induced by microwave radiation. When the photon energy of microwaves $h\nu$ (ν is the microwave frequency) is equal to the splitting ΔE, i.e. at the resonance condition, the transition occurs. In principle, the resonance condition can be satisfied by keeping the magnetic field constant while sweeping the microwave frequency or vice versa. In practice, it is easier to keep the microwave frequency fixed and to scan the magnetic field.

In thermal equilibrium, the population of electrons on the lower energy state, N_{down}, will be higher than the population of the upper state, N_{up}. The difference in the population depends on the splitting and temperature as described statistically by the Boltzmann distribution:

$$N_{down} - N_{up} = N_{tot}\frac{1-e^{-\Delta E/k_B T}}{1+e^{-\Delta E/k_B T}}$$

(3)

where $N_{tot}=N_{down}+N_{up}$.

When the microwaves induce transitions at the resonance frequency there will, in the case shown in Figure 2.1, be a net absorption of microwaves due to the population difference. (In the case of inverted population induced for example by optical excitation, a net microwave emission is detected by EPR.)

With the absorption the population would quickly be equalized, if it were not for the spin-lattice relaxation that tends to restore the thermal equilibrium conditions. This relaxation involves energy exchange between the spins and surrounding (the crystal lattice in the case of SiC) and the more efficient energy exchange the shorter the spin-lattice relaxation time, τ_1 (Ref. [53], p. 305). Several mechanisms can be involved in this relaxation (direct phonon interaction, Raman processes, etc. [54]) and it can be different for different EPR centers in the same material. A large τ_1 can lead to a reduced and distorted EPR-signal by so called saturation, and a small τ_1 leads to lifetime broadening of the EPR-signal, due to the Heisenberg uncertainty principle (Ref. [53], p. 305), which can be as bad as to make the signal undetectable.

2.2 Experimental Technique

The majority of our EPR measurements have been performed on an X-band (~9.5 GHz) Bruker ELEXSYS E580 EPR spectrometer. A schematic picture of the instrument set up with a standard cavity and a finger dewar is shown in Figure 2.2.
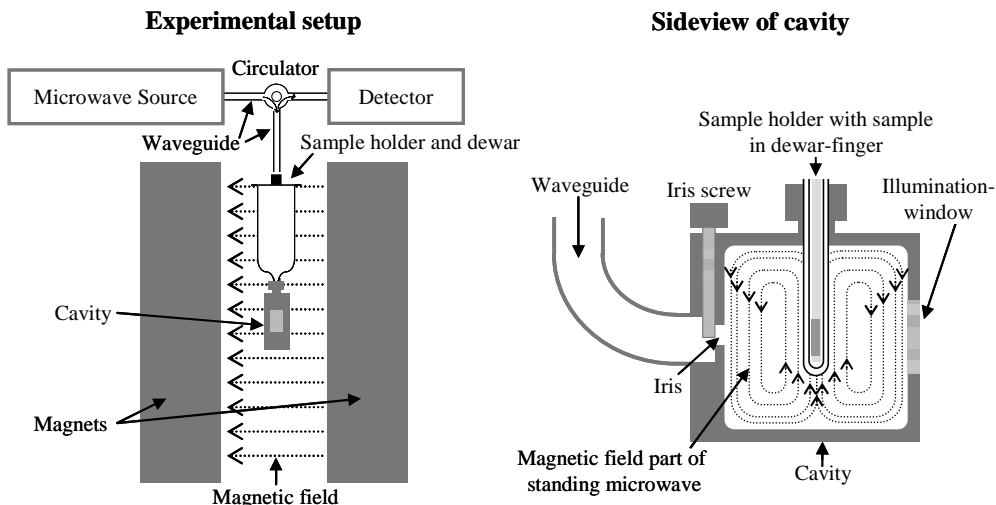

Figure 2.2 Schematic picture of the main components of an experimental setup for EPR and a cut-through side view of the cavity. In this setup, the sample is attached to a quartz rod sample holder and placed in the finger of a dewar filled with liquid nitrogen for measurements at 77 K. The sample is situated in the middle of the cavity where the magnetic field part of the standing microwave has a maximum and the electric field part has a minimum. The illumination window is for photo-EPR. For measurements at variable temperatures, a continuous He-flow cryostat is used.

With this setup, measurements can be performed at room temperature or, with the dewar filled with liquid nitrogen, at 77 K. For measurements at variable temperatures (4-300 K), a helium-flow cryostat is used.

The sample is placed in the middle of a cavity, which in turn is placed in the magnetic field (**B**). Microwaves are created in the microwave bridge (in our case by a klystron) and led to the cavity by the waveguide. The microwave is coupled into and out of the cavity through a small hole (iris) and the microwave absorption and reflection are optimized using an iris screw. The microwave frequency is tuned to create a standing wave in the cavity. The cavity is shaped so that the magnetic field part of the standing microwave is perpendicular to **B** and has a maximum in the middle of the cavity where the electric field part has a minimum. This is where the sample is placed. The standing wave frequency is determined by the size of the cavity. The microwaves not dissipated in the cavity (or in the wave guide) are reflected back in the waveguide, separated from the incoming microwaves by a circulator to be led, instead of back to the klystron, to a detector. The detector typically consists of a diode that converts the microwave signal to an electrical

current and electrical filters and amplifiers. To have the diode working in a range where there's a linear response between the intensity of the microwaves and the diode current (at ~200 μA), the diode can be biased by microwaves led directly from the klystron to the detector by a reference arm.

The magnetic field is swept with increasing field and when the level splitting caused by the field reaches hv, the transition is induced between the energy levels. At this resonance condition there is a change of microwave absorption or emission and an EPR signal is detected. In detecting an EPR spectrum, B is swept in discrete steps, and the signal intensity is measured in a number of points over the magnetic field range of interest. In order to use the lock-in technique to increase the signal-to-noise ratio, the magnetic field is modulated with a sinusoidal oscillation of a chosen frequency, as illustrated in Figure 2.3. This is done with additional coils near the
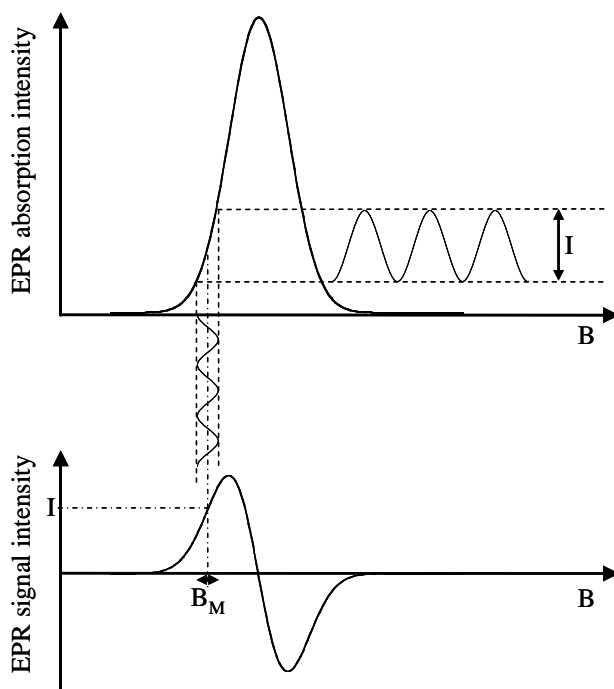
Figure 2.3 The EPR signal from detection of an absorption peak. The amplitude, I, of the signal, which oscillates due to the magnetic field modulation, is detected.

cavity, driven by the amplified signal of an oscillator. The oscillator signal is also sent to the detector to enable selective amplification of this frequency by mixing the diode signal and the oscillator signal. By tuning the phase of one of the signals so that the signals are in phase the amplified output can be optimized. This improves the signal to noise ratio substantially. The amplitude of the oscillating signal (I in Figure 2.3), corresponding to the slope of the absorption curve, is detected and therefore the EPR signal appears as the first derivative of the absorption spectrum.

The EPR sensitivity increases with the amplitude of the magnetic field modulation, B_M, (to a certain limit) but if B_M is not a small fraction of the line width of the signal, the shape of the signal is distorted.

2.3 Anisotropy

The electron energy terms relevant for EPR can be described by the Hamiltonian:

$$H = \mu_B \mathbf{BgS} + \mathbf{SDS} + \sum_i (\mathbf{SA_iI_i} - \mu_n \mathbf{Bg_{ni}I_i}) \qquad (4)$$

The first term is the electron Zeeman interaction. The second term represents the spin–spin interaction for the total electron spin $S \geq 1$, i.e. if the paramagnetic center has more than one unpaired electron spin. The terms under summation represent the interactions involving nuclear spins, the hyperfine (hf) interaction and the nuclear Zeeman interaction, where the nuclear magneton $\mu_n = e\hbar/2m_p = 3.152 \times 10^{-8}$ eV/T ($\approx \mu_B /1840$). The nuclear Zeeman effect is usually small compared to other terms and does not cause any shift for the EPR lines in the first order, so it can usually be ignored. In general cases, $\mathbf{g}$, $\mathbf{D}$ and $\mathbf{A}$ are tensors, describing anisotropic interactions which are unique for each EPR center. This makes EPR a powerful technique for identification of defects and investigation of their electronic structure. The spin-Hamiltonian parameters can be obtained from the analysis of the angular dependence of the EPR spectrum on one or several high-symmetric planes.

2.3.1 The g-tensor

It is usual for defects in single crystals that the orbital angular momentum is quenched and the total angular momentum is just the spin. The anisotropy of the $\mathbf{g}$-tensor often depends on the local symmetry of the defect.
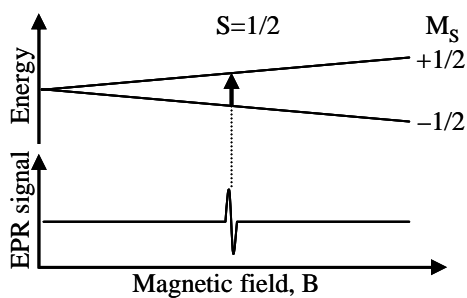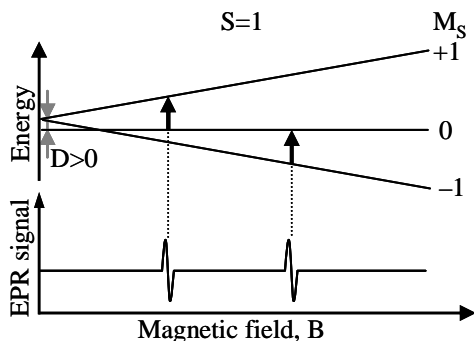

**Figure 2.4** The energy levels and EPR spectrum of a S=1/2 center.
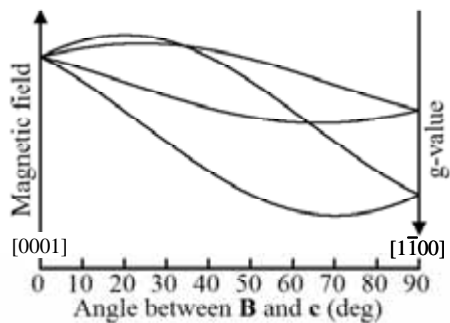
Figure 2.5 The angular dependence for rotation in the $(11\bar{2}0)$ or equivalent plane of a spin S=1/2 center in a single crystal with hexagonal lattice.

For a spin S=1/2 center without hf interaction, the first term alone of Eq. 4 is sufficient to describe the angular dependence. Figure 2.4 shows the energy scheme and the EPR signal observed at resonance. In a hexagonal lattice, for the magnetic field along the *c*-direction (**B**∥**c**), all the six possible defect orientations in the hexagonal lattice are equivalent, giving rise to the same resonance and hence only one EPR line is observed (Figure 2.5). When rotating the magnetic field away from the *c*-axis in the (11$\bar{2}$0)-plane, four of the six defect orientations become inequivalent and the corresponding resonances give rise to four separate EPR lines. The number of lines reduces to two at **B**⊥**c**. The maximum number of four lines indicates that there are two pairs of defect orientations that are equivalent. This can happen only if two principal axes, g_{xx} and g_{zz}, are lying in the (11$\bar{2}$0)-plane, i.e. the symmetry of the defect is C_{1h}. The **g**-tensor can be obtained from the fit of the angular dependence using spin-Hamiltonian Eq. 4.

2.3.2 Spin-spin interaction and the D-tensor

**Figure 2.6** The energy levels, allowed transitions, and EPR spectrum of a S=1 center with D>0.
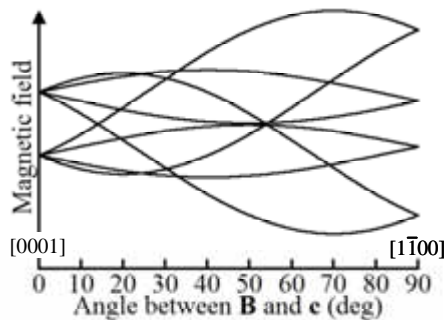
Figure 2.7 The angular dependence for rotation in the (11$\bar{2}$0) or equivalent plane of a S=1 center in a hexagonal lattice with an isotropic g-value. The angle corresponding to the direction with the largest splitting (70° from the *c*-axis in this case) defines the principle *z*-axis of the **D**-tensor.

For a defect with an electron spin S=1 there are two electrons with the same spin polarization. In such a system, there will be a dipole-dipole interaction between the two electron spins. The coupling between the spins gives rise to three states with the magnetic quantum numbers M_S = –1, 0 and 1. The singlet state (M_S=0) and the doublet state (M_S=±1) can be split up by the crystal field in absence of an external magnetic field. Such a splitting is called the zero-field splitting. Under an applied magnetic field, the doublet state splits and the three states of the system are separated (Figure 2.6). There are three possible transitions between the levels, but only the two with ΔM_S=±1 are allowed. Without zero-field splitting, both

transitions will occur at the same magnetic field and the resulting EPR spectrum will have only one line. With zero-field splitting, these transitions will occur at two different magnetic fields, as shown in Figure 2.6. Depending on the crystal structure and the geometry of the defect, the zero-field splitting is usually anisotropic and described by the **D**-tensor. Figure 2.7 shows the angular dependence of the EPR spectrum for a S=1 center in a hexagonal lattice with an isotropic g-value and C_{1h} symmetry. In this case, the anisotropy is caused by the anisotropy of the **D**-tensor. **D** is a traceless tensor with $D_{zz}+D_{xx}+D_{yy}=0$ and is commonly described by the fine-structure parameters D and E which are defined as $D=3D_{zz}/2$, and $E=(D_{xx}-D_{yy})/2$. D and E are the fine-structure parameters representing the zero-field splitting due to the axial and orthorhombic crystal fields, respectively. The **D**-tensor can be obtained from the fit to the angular dependence using the spin-Hamiltonian in Eq. 4 (including the first and second terms). The angle corresponding to the direction with the largest splitting of the EPR spectrum defines the principal *z*-axis of the **D**-tensor.

2.3.3 Hyperfine interaction and the A-tensor

For an impurity with a nucleus having a nuclear spin I≠0 there will be an interaction between the electron spin and the nuclear spin. This interaction is called the hf interaction and is described by the third term in Eq. 4. Unpaired electrons may also localize on neighboring atoms. If the host atoms have nuclear spins different from zero, there will also be hf interaction between the electron spin and the nuclear spins of neighboring nuclei. The strength and the anisotropy of the interaction depend on the distribution of the spin at the defect and surrounding.
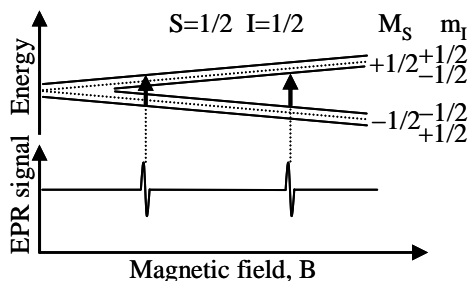

Figure 2.8 The energy levels and EPR spectrum of an impurity with an electron spin S=1/2 having only one isotope (i.e, 100% natural abundance) with a nuclear spin I=1/2.
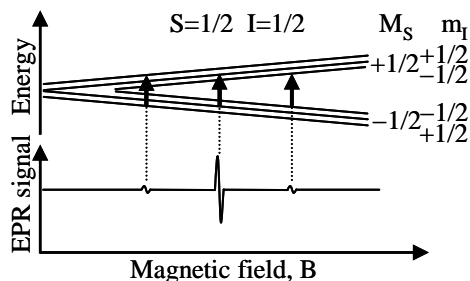
Figure 2.9 The energy levels and EPR spectrum of an impurity with S=1/2 having two isotopes, one with ~10% natural abundance and I=1/2 and the other with ~90% natural abundance and I=0.

Figure 2.8 shows the energy scheme levels for a center with an electron spin S=1/2 and a nuclear spin I=1/2. The external magnetic field splits first the level into two levels with $M_S=\pm1/2$ by the Zeeman effect (dotted lines in Figure 2.8). The hf interaction will further split each $M_S=-1/2$ and $M_S=+1/2$ states into two levels corresponding to the nuclear quantum number $m_I=+1/2$ and $m_I=-1/2$. Commonly, the hf splitting is much smaller than the electronic Zeeman splitting and only the

transitions with $\Delta M_S = \pm 1$, $\Delta m_I = 0$ are allowed. Thus, this center will give rise to an EPR spectrum with two lines as shown in the lower part of Figure 2.8. Among the different silicon isotopes, only [29]Si has a nuclear spin different from zero (I=1/2). Its natural abundance is ~4.7%. For carbon only the ^{13}C isotope has a non-zero nuclear spin (I=1/2); its natural abundance is small (~1.1%). Thus, the hf interaction with a Si- or C-atom gives rise to an EPR spectrum consisting of three lines similar to the one shown in Figure 2.9. However, the [29]Si hf lines will have about four times higher intensity (~4.7% of the intensity of the central line) compared to the ^{13}C hf lines (~1.1% of the intensity of the main line). Thus, from the number of lines the nuclear spin can be determined while the intensity ratio between the hf lines and the main line provides the information on the natural abundance of the isotope. Such information allows for the chemical identification of the involved impurity.
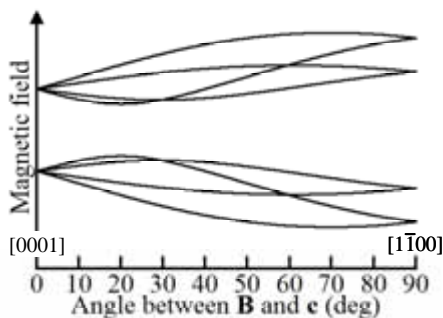

Figure 2.10 The angular dependence of the hf lines of a center in a hexagonal lattice, S=1/2 and I=1/2, and an isotropic g-value, for the magnetic field rotating in the (11$\bar{2}$0) plane from the [0001] to the [11$\bar{2}$0] direction (the main line is not shown).

The angular dependence of the hf lines with an isotropic g value and an anisotropic hf interaction is illustrated in Figure 2.10. The principal A-values can be obtained from the fit of the angular dependence using proper terms in the spin-Hamiltonian Eq. 4.

2.4 Photoexcitation-EPR

For an EPR active defect, illumination with proper photon energies can excite electrons to the defect level or remove them from it. As a result, a part of the total defect concentration is changed into other charge states which are EPR inactive. This induces changes in the EPR signal. In this way, a defect that is in an EPR inactive charge state in darkness can be more or less activated by illumination to an EPR active charge state. This is called photoexcitation EPR (photo-EPR). Using monochromatic light from a monochromator or a tunable laser, photo-EPR can also provide information on the location in the band gap of the energy levels of a defect. By plotting the change in EPR intensity for an EPR-center vs. the photon energy the threshold energy, when the intensity starts increasing or decreasing, corresponds to

the photoexcitation to a level from the valence band (E_V) or from a level to the conduction band (E_C). Examples of results from this technique can be found in Papers 2, 4 and 5. The interpretation of these results are, however, complicated by possible inter-level transitions, i.e. the transitions are not from E_V or to E_C but between defect levels, especially if there are many other defect levels in the sample. In some cases, when the Franck-Condon shifts [55,56] are not negligible, the optical transitions corresponding to the energy thresholds determined from photo-EPR may not correspond to the ionization energies between the defect levels or between the level and the band edges measured in equilibrium. As illustrated in the configuration coordinate (Q) vs. energy (E) diagram in Figure 2.11, optical transitions, being instantaneous in the time scale of nuclear movements, are most likely vertical in the diagram. The actual energy difference, ΔE in Figure 2.11, can therefore be smaller than the optical transition energy, if the atomic positions in the defect are not exactly the same for different charge states. The energy threshold in photo-EPR gives the optical transition energy, which can be larger than the ionization energy determined by e.g. DLTS in equilibrium by an unknown amount.
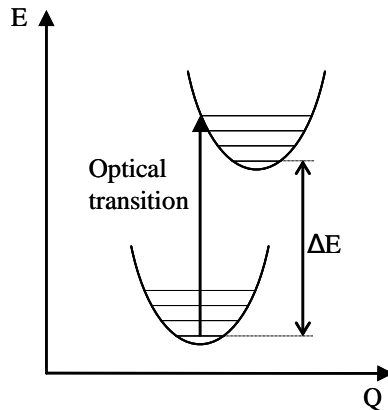
Figure 2.11 Optical transition between two electronic charge states in the configuration coordinate model. The horizontal lines are vibronic levels. The Franck-Condon shift is the difference between the optical transition energy and ΔE, the energy difference between the lowest vibronic levels of the two states.

References

[1] J. J. Berzelius, Annalen der Physik und Chemie, Leipzig 1, 169 (1824).

[2] H. Moissan, Comptes Rendus Hebdomadaires des Séances de l'Académie des Sciences 140, 405 (1905).

[3] E. G. Acheson, English Patent No. 17911 (1892).

[4] J. A. Lely, Berichte der Deutschen Keramischen Gesellschaft 32, 229 (1955).

[5] Y. M. Tairov and V. F. Tsvetkov, J. Cryst. Growth 43, 209 (1978).

[6] H. Matsunami, S. Nishino, and H. Ono, IEEE Transactions on Electron Devices 28, 1235 (1981).

[7] R. F. Davis, Institute of Physics Conference Series 137, 1 (1994).

[8] L. S. Ramsdell, American Mineralogist 32, 64 (1947).

[9] W. F. Knippenberg, Philips Research Reports 18, 161 (1963).

[10] H. Wingrant, Studies on MISiC-FET sensors for car exhaust gas monitoring, Dissertation thesis No. 931, Linköping University, Linköping (2005).

[11] A. Salomonsson, New materials for gas sensitive field-effect device studies, Dissertation thesis No. 957, Linköping University, Linköping (2005).

[12] M. Andersson, SiC based field effect sensors and sensor systems for combustion control applications, Dissertation thesis No. 1077, Linköping University, Linköping (2005).

[13] W. J. Choyke, D. R. Hamilton, and L. Patrick, Phys. Rev. 133, A1163 (1964).

[14] R. F. Davis, Proc IEEE 79, 702 (1991).

[15] A. Qteish, V. Heine, and R. J. Needs, Phys. Rev. B Condens. Matter Mater. Phys. 45, 6534 (1992).

[16] H. Morkoç, S. Strite, G. B. Gao, M. E. Lin, B. Sverdlov, and M. Burns, J. Appl. Phys. 76, 1363 (1994).

[17] www.cree.com

[18] V. E. Chelnokov and A. L. Syrkin, Mater. Sci. Eng. B 46, 248 (1997).

[19] A. A. Lebedev and V. E. Chelnokov, Semiconductors 33, 999 (1999).

[20] A. Schönflies, Krystallsysteme und Krystallstructur, edited by B. G. Teubner , Leipzig, (1891).

[21] E. Janzén, A. Gali, A. Henry, I. G. Ivanov, B. Magnusson, and N. T. Son, Defects in SiC (Taylor and Francis LLC, 2008), p. 615.

[22] M. Bockstedte, M. Heid, and O. Pankratov, Phys. Rev. B Condens. Matter Mater. Phys. 67, 1931021 (2003).

[23] N. T. Son, P. N. Hai, and E. Janzén, Phys. Rev. B Condens. Matter Mater. Phys. 63, 2012011 (2001).

[24] T. Umeda, J. Isoya, N. Morishita, T. Ohshima, and T. Kamiya, Phys. Rev. B Condens. Matter Mater. Phys. 69, 1212011 (2004).

[25] V. Y. Bratus', T. T. Petrenko, S. M. Okulov, and T. L. Petrenko, Phys. Rev. B Condens. Matter Mater. Phys. 71, 1 (2005).

[26] T. Umeda, Y. Ishitsuka, J. Isoya, N. T. Son, E. Janzén, N. Morishita, T. Ohshima, H. Itoh, and A. Gali, Phys. Rev. B Condens. Matter Mater. Phys. 71, 1 (2005).

[27] T. Umeda, J. Isoya, N. Morishita, T. Ohshima, T. Kamiya, A. Gali, P. Deák, N. T. Son, and E. Janzén, Phys. Rev. B Condens. Matter Mater. Phys. 70, 1 (2004).

[28] A. Zywietz, J. Furthmüller, and F. Bechstedt, Phys. Rev. B Condens. Matter Mater. Phys. 59, 15166 (1999).

[29] L. Torpo, R. M. Nieminen, K. E. Laasonen, and S. Pöykkö, Appl. Phys. Lett. 74, 221 (1999).

[30] L. Torpo, M. Marlo, T. E. M. Staab, and R. M. Nieminen, J. Phys.: Condens. Matter 13, 6203 (2001).

[31] T. Wimbauer, B. K. Meyer, A. Hofstaetter, A. Scharmann, and H. Overhof, Phys. Rev. B Condens. Matter Mater. Phys. 56, 7384 (1997).

[32] J. Schneider and K. Maier, Physica B: Physics of Condensed Matter 185, 199 (1993).

[33] V. S. Vainer and V. A. Il'in, Sov. Phys. Solid State 23, 2126 (1981).

[34] N. T. Son, P. Carlsson, J. ul Hassan, et al, Phys. Rev. Lett. 96, 055501 (2006).

[35] M. Bockstedte, A. Mattausch, and O. Pankratov, Phys. Rev. B Condens. Matter Mater. Phys. 68, 2052011 (2003).

[36] E. Rauls, T. Frauenheim, A. Gali, and P. Deák, Phys. Rev. B Condens. Matter Mater. Phys. 68, 1552081 (2003).

[37] T. Umeda, J. Ishoya, T. Ohshima, N. Morishita, H. Itoh, and A. Gali, Phys. Rev. B Condens. Matter Mater. Phys. 75 (2007).

[38] T. Umeda, N. T. Son, J. Isoya, E. Janzen, T. Ohshima, N. Morishita, H. Itoh, A. Gali, and M. Bockstedte, Phys. Rev. Lett. 96, 145501 (2006).

[39] N. T. Son, P. Carlsson, J. Ul Hassan, B. Magnusson, and E. Janzén, Phys. Rev. B Condens. Matter Mater. Phys. 75 (2007). -Paper 1 in this thesis

[40] P. Carlsson, N. T. Son, B. Magnusson, A. Henry, and E. Janzén, Mater. Sci. Forum 600-603, p. 381 (2009). -Paper 4 in this thesis

[41] H. M. Hobgood, R. C. Glass, G. Augustine, R. H. Hopkins, J. Jenny, M. Skowronski, W. C. Mitchel, and M. Roth, Appl. Phys. Lett., 1364 (1995).

[42] A. P. Zhang, L. B. Rowland, E. B. Kaminsky, et al, J. Electron Mater. 32, 437 (2003).

[43] N. T. Son, P. Carlsson, A. Gällström, B. Magnusson, and E. Janźn, Appl. Phys. Lett. 91 (2007).

[44] N. Achtziger and W. Witthuhn, Phys. Rev. B Condens. Matter Mater. Phys. 57, 12181 (1998).

[45] A. Ellison, B. Magnusson, C. Hemmingsson, W. Magnusson, T. Iakimov, L. Storasta, A. Henry, N. Henelius, and E. Janzén, Mater. Res. Soc. 640, p. H1.2.1. (2001).

[46] A. Ellison, B. Magnusson, N. T. Son, L. Storasta, and E. Janzén, Mater. Sci. Forum 433-436, p. 33. (2003)

[47] A. Ellison, B. Magnusson, B. Sundqvist, G. Pozina, J. P. Bergman, E. Janzén, and A. Vehanen, Mater. Sci. Forum 457-460, p. 9. (2004).

[48] S. G. Müller, M. F. Brady, W. H. Brixius, et al, Mater. Sci. Forum 433-436, p. 39. (2003)

[49] J. R. Jenny, D. P. Malta, M. R. Calus, S. G. Müller, A. R. Powell, V. F. Tsvetkov, H. M. Hobgood, R. C. Glass, and C. H. Carter Jr., Mater. Sci. Forum 457-460, p. 35. (2004).

[50] E. Zavoisky, J. Phys. U. S. S. R. 9, 211 (1945).

[51] E. Zavoisky, J. Phys. U. S. S. R. 9, 245 (1945).

[52] P. Zeeman, Nature 55, 347 (1897).

[53] J. A. Weil and J. R. Bolton, Electron paramagnetic resonance : elementary theory and practical applications (Wiley, Hoboken, N.J., 2007), p. 664.

[54] A. G. Redfield, Adv. Magn. Reson. 1, 1 (1965).

[55] J. Franck, Trans. Faraday Soc. 21, 536 (1925).

[56] E. U. Condon, Phys. Rev. 32, 858 (1928).